

**Integrating superior conductivity and active sites: Fe/Fe<sub>3</sub>C@GNC as trapping-catalyst interlayer and dendrite-free lithium host for lithium-sulfur cell with eminent rate performance**

**Experimental Section**

**Materials:** Commercial melamine foam (MF) was purchased from SINOYQX Co. Ltd., Sichuan, China. pyrrole monomer (Aladdin, 99.8%), FeCl<sub>3</sub>·6H<sub>2</sub>O (Aladdin, 99.8%) and other reagents were of analytical grade and directly used without further purification.

**Synthesis of Fe/Fe<sub>3</sub>C@GNC:** To start with, 3 pieces 4×4×1 cm<sup>3</sup> commercial melamine foam (MF) were soaked in aqueous pyrrole monomer solution (50 mmol/L), then sonicated for 20 minutes to make sure pyrrole monomer was homogeneously attached to MF. A FeCl<sub>3</sub>·6H<sub>2</sub>O solution of double molarity was subsequently slowly dropped into as-prepared solution with constant agitation in the ice bath, which the polymerize procedure lasted for 10 hours. After white MF covered all over with black polypyrrole (PPy), took it out and dried in a 70 °C vacuum for 24 hours. The final step, the dried product was pyrolyzed at 1000 °C for 1 hour under argon atmosphere to gain the Fe/Fe<sub>3</sub>C@GNC composite with a heating rate of 5 °C min<sup>-1</sup>.

**Separator modification:** The Fe/Fe<sub>3</sub>C@GNC interlayer was prepared by mixing 90 wt% Fe/Fe<sub>3</sub>C@GNC, 10 wt% PVDF (polyvinylidene fluoride) and grinded for 30 minutes, then the evenly mixed powder was dispersed in NMP (1-methyl-2-pyrrolidinone) and stirred vigorously to obtain homogeneous slurry. After that, the prepared slurry was uniformly coated on a commercial Celgard 2400 (PP) separator with a doctor blade and dried at 60 °C overnight. Finally, the functionalized separator was cut into slices with a diameter of 18 mm. The Fe/Fe<sub>3</sub>C@GNC interlayer has a thickness of about 15 μm, and mass loading of 1.7 mg cm<sup>-2</sup>. The carbon backbone (CB) modified separator was prepared by the same procedure using carbonized MF powder instead of Fe/Fe<sub>3</sub>C@GNC powder. The CB layer is of equivalent mass loading with Fe/Fe<sub>3</sub>C@GNC interlayer, with a thickness of 53 μm.

**Characterization of materials:** X-ray diffraction (XRD) patterns were carried out on a Bruker D8 ADVANCE diffractometer with Cu K $\alpha$  radiation in the range of 10° to 70°. The Brunauer-Emmett-Teller (BET) surface area was obtained on a Tristar II 3020 instrument. The morphology and microstructure were pictured using Field-emission scanning electron microscopy (FESEM, FEI Inspect F50) operating at 10 KV. Transmission electron microscope (TEM) equipped with a selected area electron diffraction (SAED) system was conducted to characterize the inner morphology and crystalline structure of materials with FEI Talos F200x, X-ray photoelectron spectroscopy (XPS, AXIS Ultra DLD, Kratos) was performed to determine the surface element composition and chemical bond characteristics. The graphitization extent of carbon was analyzed via Raman spectroscopy on a Lab RAM HR spectrometer (HORIBA Jobin Yvon S.A.S.) with a He-Ne laser at 633 nm in the wavenumber range of 800-2000 cm<sup>-1</sup>. Thermogravimetric analysis (TGA) was acquired on a simultaneous TGA/DSC-2 instrument (METTLER TOLEDO, USA) with a heating rate of 5 °C min<sup>-1</sup> from room temperature to 800 °C under oxygen atmosphere. The adsorption experiments of polysulfide solution were examined by UV-visible absorption spectrophotometry (UV-vis, Shimadzu UV3600). The magnetic properties of the catalysts were measured at room temperature by using a vibrating sample magnetometer (VSM, PPMS-9).

**Electrochemical measurements of modified separator:** Coin-type CR2032 cells were assembled by SP/S electrode, the modified separator and Li foil as the cathode, separator and anode, separately, in a glovebox filled with Ar with O<sub>2</sub> and H<sub>2</sub>O contents under 0.1 ppm. To prepare the SP@S cathode, nano sulfur, Super P and PVDF were mixed and grinded together for 30 minutes with a mass ratio of 5:4:1, then NMP was added into the uniform mixture and grinded for another 20 minutes subsequently. The obtained slurry was coated onto the carbon-coated aluminum (CA) foil and dried at 60 °C under vacuum overnight. The sulfur loading was controlled at 1.3 mg cm<sup>-2</sup> without specific illustration when coated foil was punched into 12 mm circular disks. The electrolyte was prepared by dissolving 1.0 M lithium bis(trifluoromethylsulphonyl)imide (LiTFSI, 99.95%, Sigma) with LiNO<sub>3</sub> additive of

2 wt% in a mixed solvent of 1,2-dimethoxyethane (DME) and 1,3-dioxolane (DOL) (1:1 by volume). The volume of electrolyte in one cell was about 45  $\mu\text{L}$ . Electrochemical tests were performed by a multi-channel test instrument (Neware CT-3008W, China) handled in a voltage window range of 1.7-2.8 V (vs. Li/Li<sup>+</sup>) at different current densities. Cyclic voltammetry (CV) measurements with a voltage window range of 1.7-2.8 V was conducted using a PARATAT multichannel electrochemical workstation (Princeton Applied Research, USA). Electrochemical impedance spectroscopy (EIS) was gathered within a frequency range of 0.1 Hz to 100 kHz with an applied amplitude of 5 mV using a CHI760 electrochemical measurement system.

***Assembly of Li<sub>2</sub>S<sub>6</sub> symmetric cells and kinetic characterization:*** Li<sub>2</sub>S<sub>6</sub> electrolyte (0.1 M) was prepared by mixing Li<sub>2</sub>S and S at a molar ratio of 1:5 into Li-S electrolyte. The symmetric cell for kinetic CV test was fabricated with Fe/Fe<sub>3</sub>C@GNC or CB coated CA foils as both anode and cathode (1 mg cm<sup>-2</sup>) according to the above-mentioned method. They were assembled into a CR2025 coin cell using 20  $\mu\text{L}$  of Li<sub>2</sub>S<sub>6</sub> electrolyte each side with a PP membrane as the separator. The CV curves were measured at a scan rate of 3 mV s<sup>-1</sup> in a voltage window between -1 and 1 V.

***Nucleation of Li<sub>2</sub>S on various substrates:*** The catholyte was composed of 0.3 M Li<sub>2</sub>S<sub>8</sub> and 1.0 M LiTFSI in tetraglyme solution. Fe/Fe<sub>3</sub>C@GNC and CB were coated onto CA discs with a diameter of 12 mm as working electrode with identical loading of 1 mg cm<sup>-2</sup> as good as a slice of CA as the counter electrode to assemble the coin cells. 25  $\mu\text{L}$  of Li<sub>2</sub>S<sub>8</sub> catholyte was added onto the modified electrode and 15  $\mu\text{L}$  of blank tetraglyme dropped onto the anode compartment. After standing for 6 hours, the cells were galvanostatically discharged at 0.112 mA to 2.06 V, followed by a potentiostatic step under 2.05 V to allow Li<sub>2</sub>S nucleation and growth.

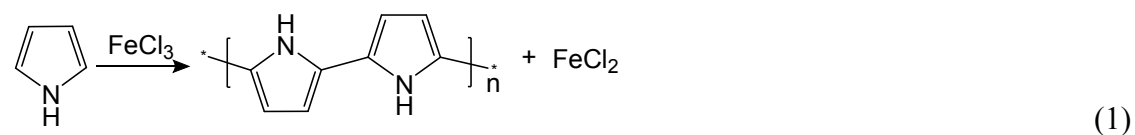
***Li metal anode tests:*** Cu@Fe/Fe<sub>3</sub>C@GNC working electrode was prepared by mixing Fe/Fe<sub>3</sub>C@GNC composite (90 wt%) and PVDF binder (10 wt%) in NMP and onto Cu foil, which was punched into a disk with a diameter of 12 mm, with mass loading of about 1.0 mg cm<sup>-2</sup>, while the lithium foil was used as the counter electrode in a CR2032 coin cell. 40  $\mu\text{L}$  of above-mentioned electrolyte was added in each cell. Assembled cells

were primarily cycled from 0 to 1 V for 5 cycles at a current density of 50  $\mu\text{A}$  to stabilize the interface.

**Li-S full cell tests:** Li-S full cell was assembled by using Li@Fe/Fe<sub>3</sub>C@GNC as anode, Fe/Fe<sub>3</sub>C@GNC coated PP as separator and SP@S as cathode (same way as ordinary cathode). The sulfur loading was controlled at 1.5 mg cm<sup>-2</sup>, while the Li@Fe/Fe<sub>3</sub>C@GNC anode was prepared by pre-plating 5 mA h cm<sup>-2</sup> of Li onto Fe/Fe<sub>3</sub>C@GNC coated Cu foil. The electrolyte was 50  $\mu\text{L}$  for each cell. The contrast sample was assembled using the identical method without Fe/Fe<sub>3</sub>C@GNC modification. The galvanostatic charge/discharge tests were performed with Neware CT-3008W tester at different current densities within a cutoff voltage window of 1.7-2.8 V

**Computational Methods:** The present first principle DFT calculations are performed with the projector augmented wave (PAW) method [1-2]. The exchange-functional is treated using the generalized gradient approximation (GGA) of Perdew-Burke-Ernzerhof (PBE)[3] functional. The cut-off energy of the plane-wave basis is set at 500 eV for optimize calculations of atoms and cell optimization. The vacuum spacing in a direction perpendicular to the plane of the catalyst is at least 12 Å. The Brillouin zone integration is performed using 4×4×1 Monkhorst-Pack k-point sampling for a primitive cell[4]. The self-consistent calculations apply a convergence energy threshold of 10<sup>-5</sup> eV. The equilibrium lattice constants are optimized with maximum stress on each atom within 0.05 eV/Å. The Hubbard U (DFT+U) corrections for 3d transition Fe metal by setting according to the literature[5]. The binding Energies is calculated as  $E_{\text{ads}} = E_{\text{total}} - E_1 - E_{\text{Li}_2\text{S}_6}$  where the  $E_{\text{total}}$  is the structure with Li<sub>2</sub>S<sub>6</sub> molecular,  $E_{\text{Li}_2\text{S}_6}$  is the energy of the Li<sub>2</sub>S<sub>6</sub> molecular,  $E_1$  is the surface energy. What's more, Li ions migration barrier energies had been evaluated using the climbing nudged elastic band (CI-NEB) methods.

The detailed reaction process was revealed by the following reaction equations.



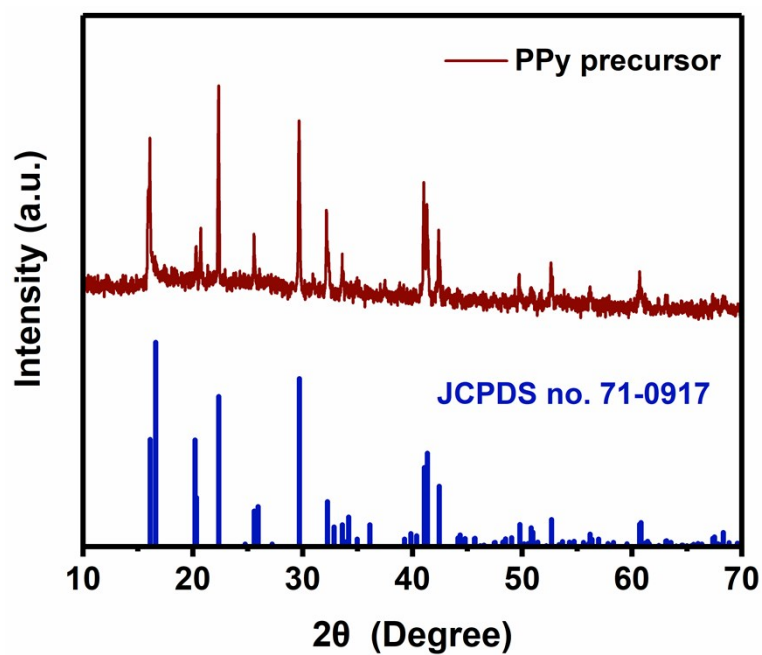


**Fig. S1** XRD patterns of PPy precursor and JCPDS card of FeCl<sub>2</sub>·4H<sub>2</sub>O.

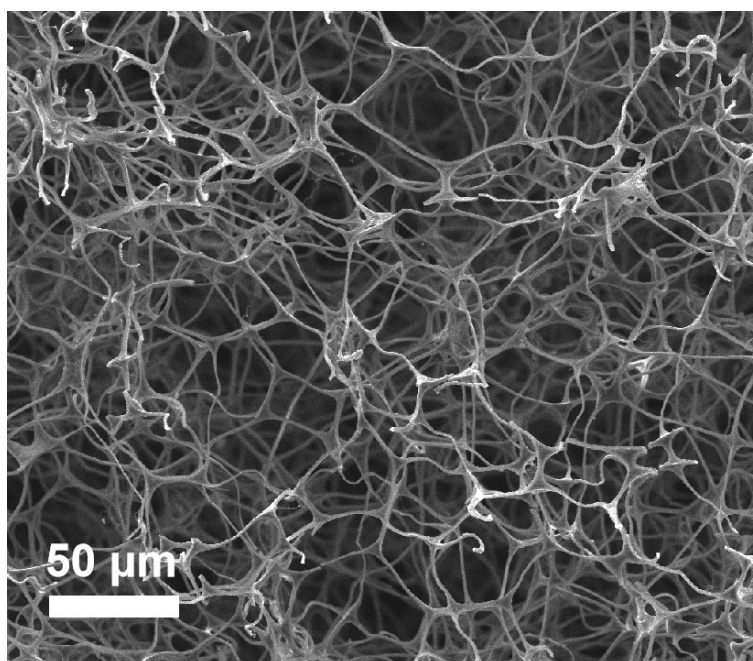


**Fig. S2** The SEM image of MF after calcination treatment at 1000 °C

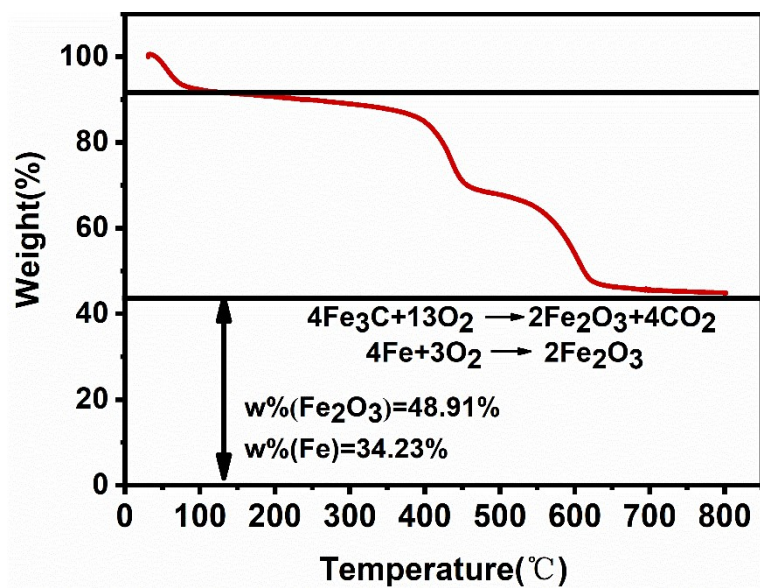


**Fig. S3** TGA curves of Fe/Fe<sub>3</sub>C@GNC under O<sub>2</sub> atmosphere from room temperature to 800 °C.

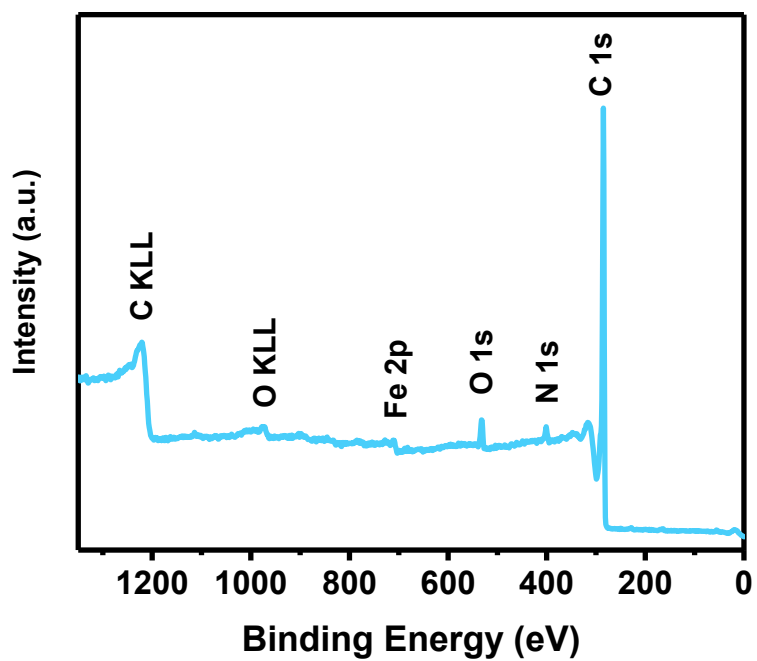


**Fig. S4** XPS survey spectra of Fe/Fe<sub>3</sub>C@GNC.

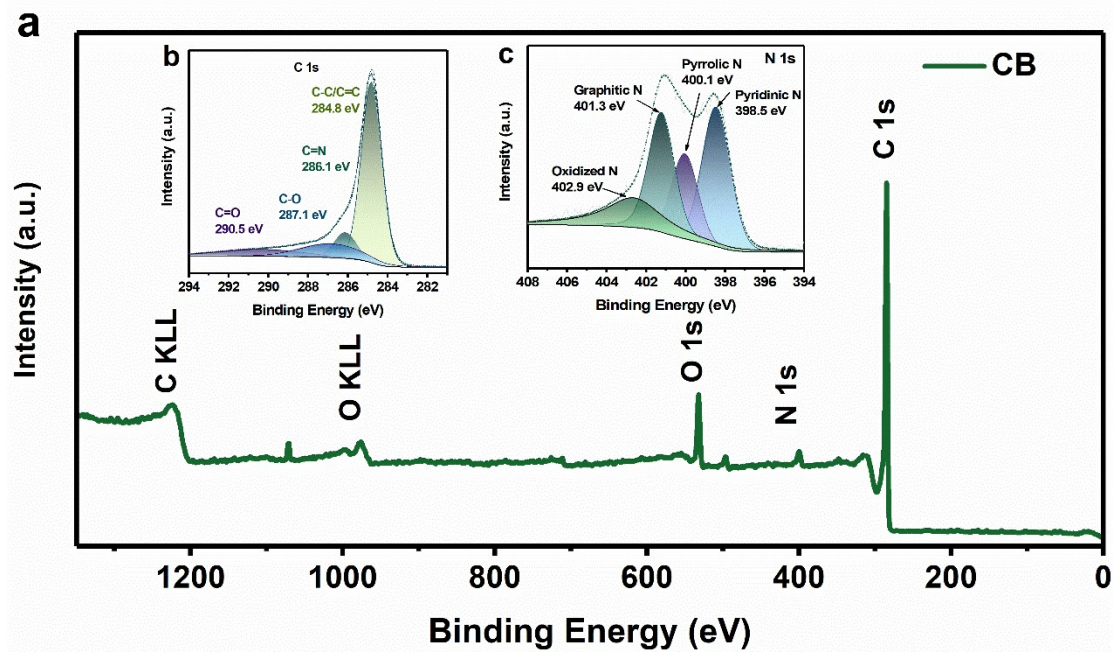


**Fig. S5** XPS spectra of CB composite and the corresponding (b) C 1s and (c) N 1s elemental XPS spectra in the insets.

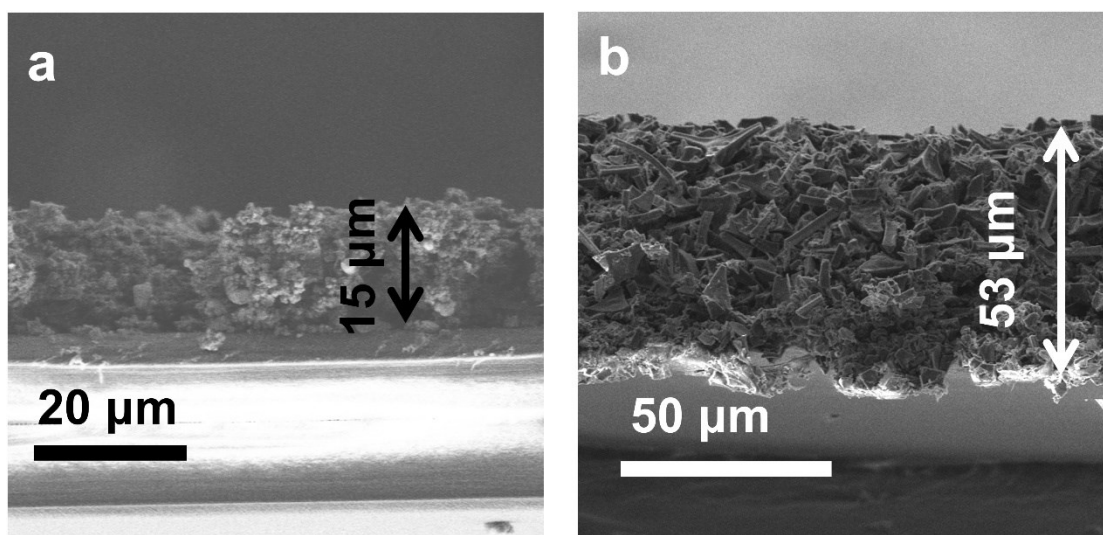


**Fig. S6** Cross-sectional SEM image of the (a) Fe/Fe<sub>3</sub>C@GNC-PP and (b) CB-PP separator.

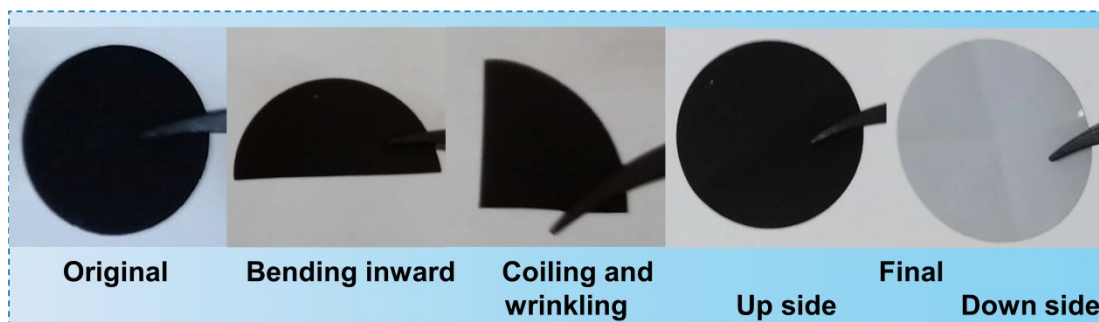


**Fig. S7** Digital photos of the Fe/Fe<sub>3</sub>C@GNC-PP separator under various mechanical stresses.

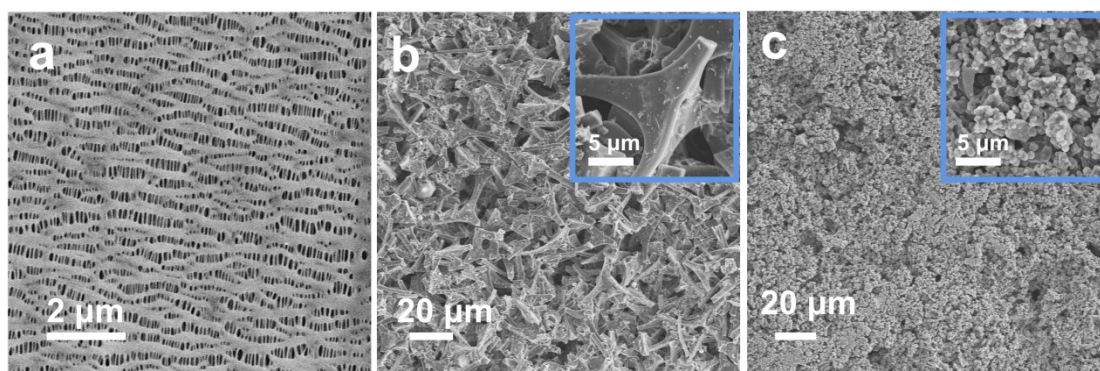


**Fig. S8** SEM images of one side of the (a) PP and (b) CB-PP and (c) Fe/Fe<sub>3</sub>C@GNC-PP separators.

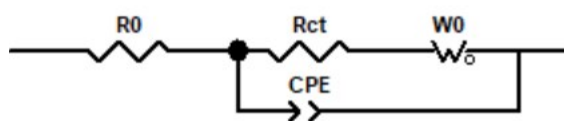


**Fig. S9** Equivalent circuit model fitted EIS curves of the Fe/Fe<sub>3</sub>C@GNC interlayer, CB interlayer and without interlayer.

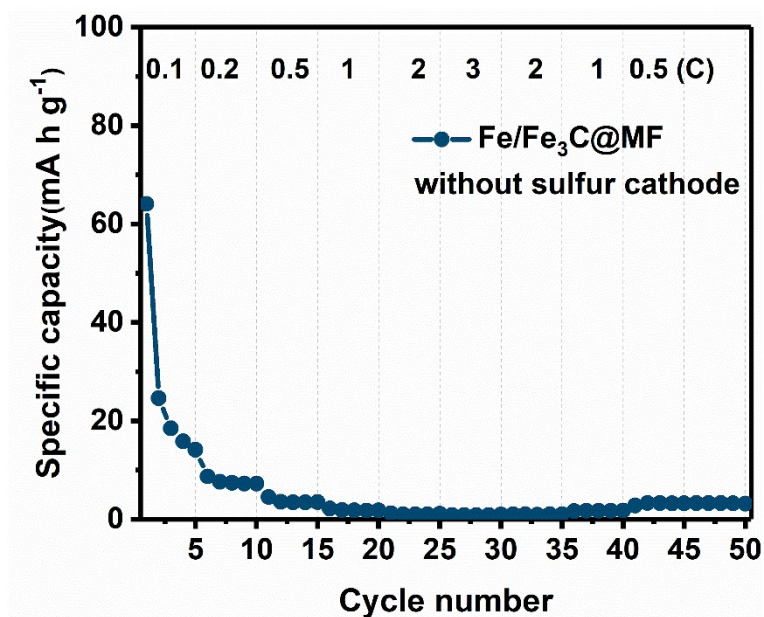


**Fig. S10** The capacity contribution of Li<sup>+</sup> insertion into Fe/Fe<sub>3</sub>C@GNC under various current rates.

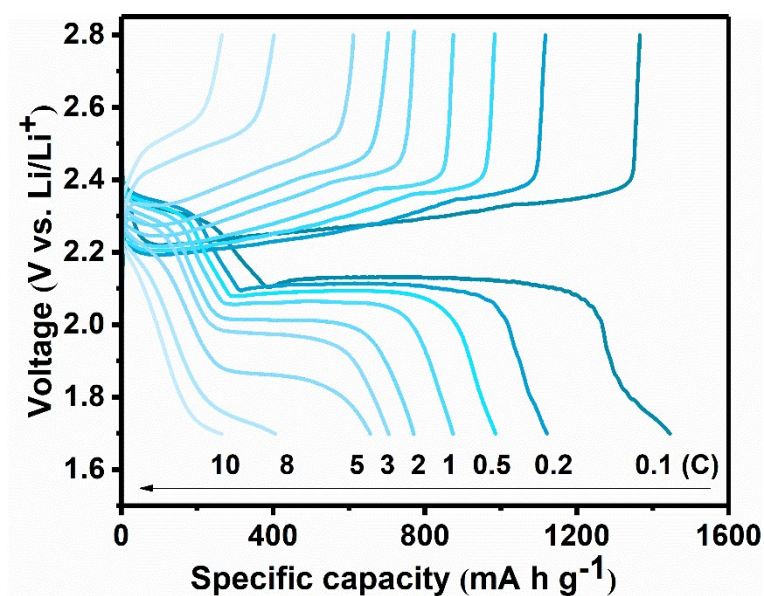


**Fig. S11** The galvanostatic charge-discharge profiles of Fe/Fe<sub>3</sub>C@GNC interlayer at various current rates.

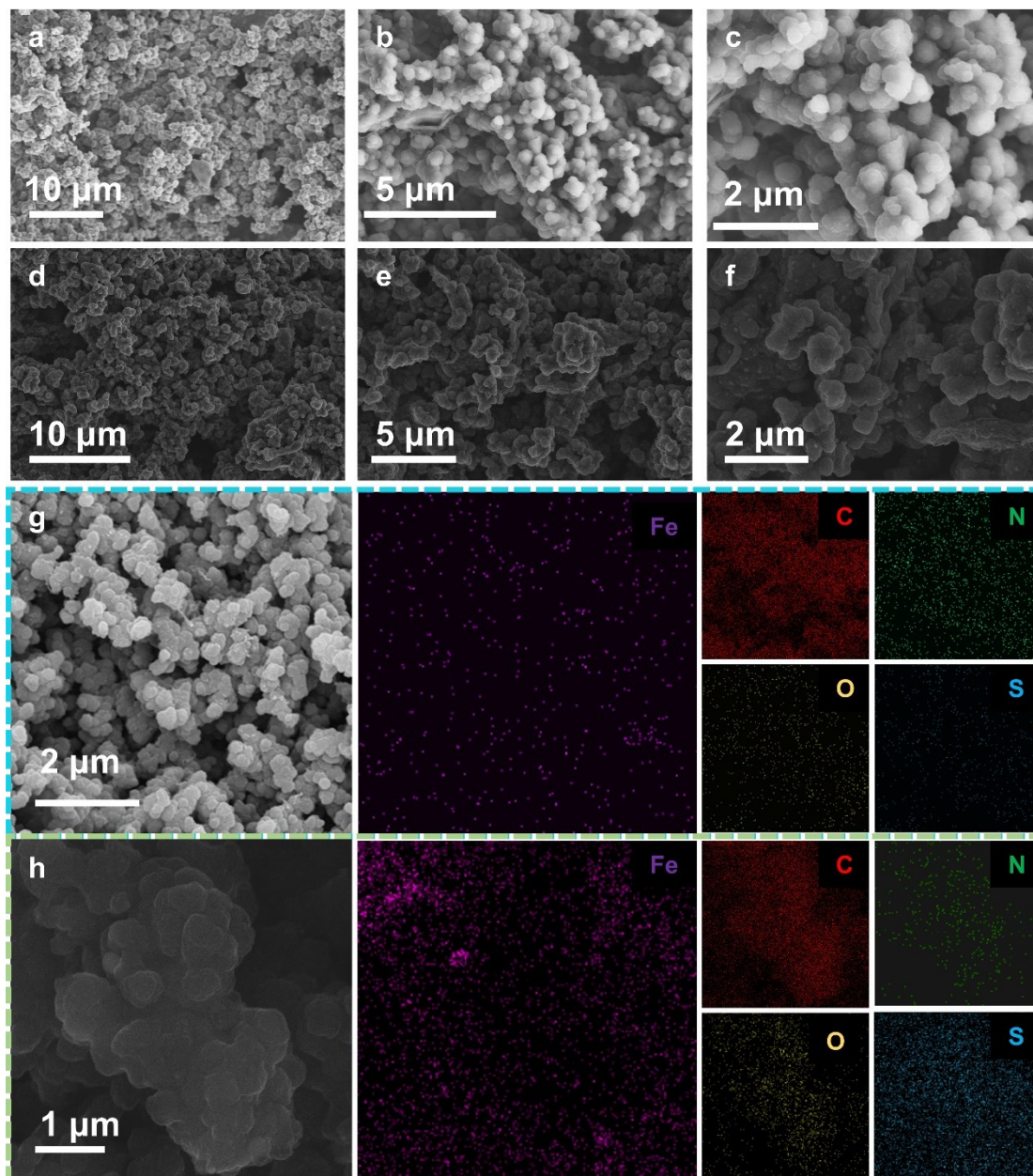


**Fig. S12** FESEM images at different magnifications of the Fe/Fe<sub>3</sub>C@GNC interlayer (a-c) before and (d-f) after 200 cycles at 1 C under 55 °C. Elemental mapping results (g) before and (h) after cycling of element Fe, C, N, O and S.

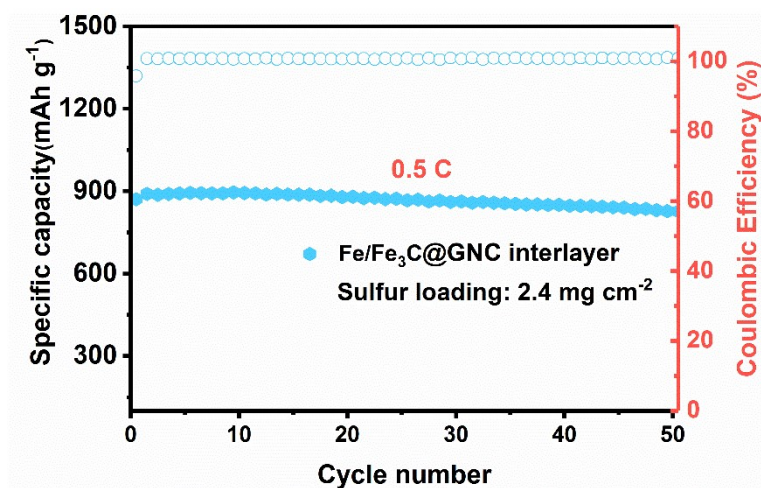


**Fig. S13** Cycling performance of Fe/Fe<sub>3</sub>C@GNC interlayer with sulfur loading of 2.4 mg cm<sup>-2</sup> at 0.5 C.

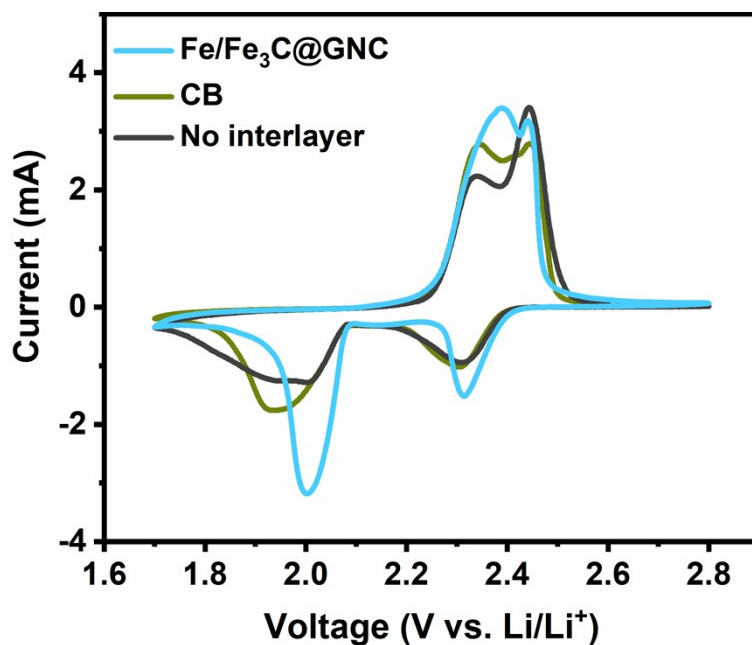


**Fig. S14** CV curves of cells with three various samples at a scan rate of 0.1 mV s<sup>-1</sup> in the second cycle.

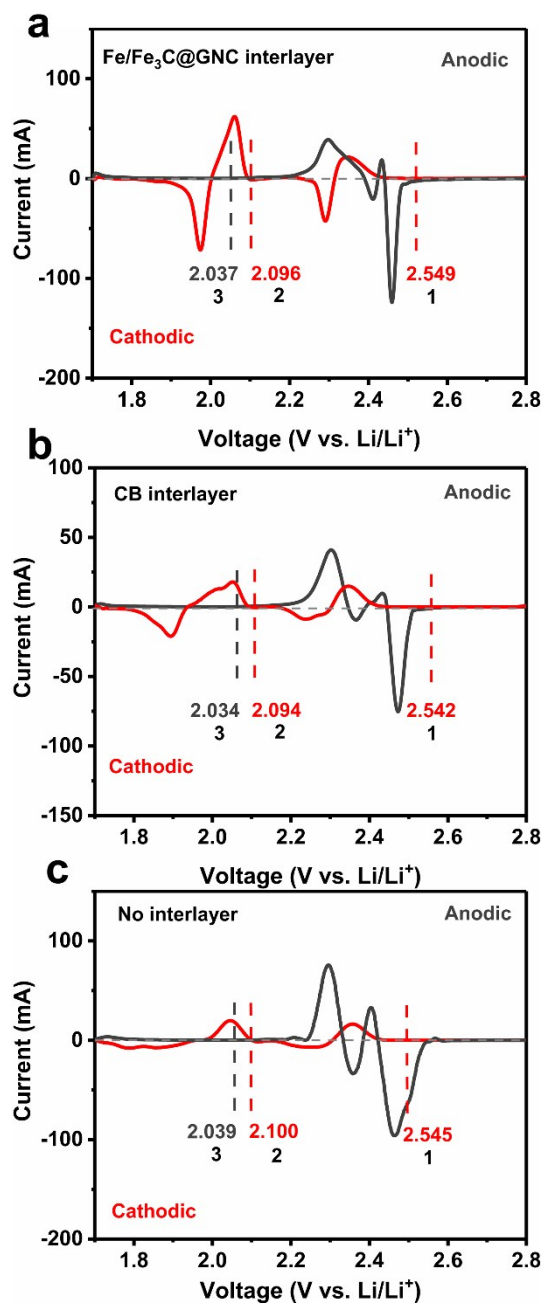


**Fig. S15** Electrocatalytic effects of electrode materials verified from the CV profiles: differential CV curves of (a) Fe/Fe<sub>3</sub>C@GNC, (b) CB and (c) without interlayer.

The baseline potentials and baseline current densities in (a, b, c) are defined as the values before the redox peaks, where the variation on current density is the smallest, namely  $dI/dV=0$ . Baseline voltages are denoted in red for cathodic peak 1, 2 and in black for anodic peak 3, respectively.

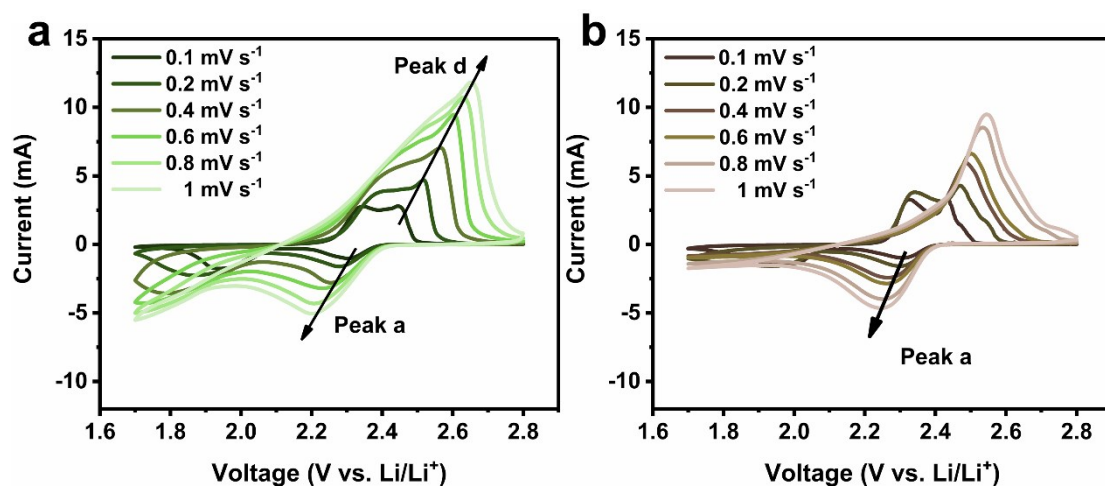


**Fig. S16** Typical CV curves of Li-S cells with (a) CB interlayer and (b) pure PP at different scan rates.

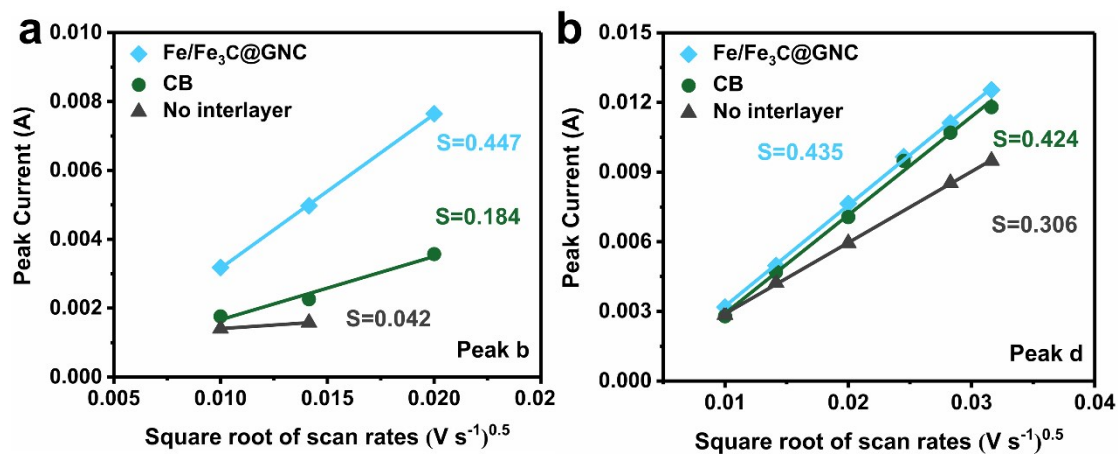


**Fig. S17** CV peak current for the (a) second cathodic reduction process (peak b:  $\text{Li}_2\text{S}_x \rightarrow \text{Li}_2\text{S}$ ,  $4 \leq x \leq 8$ ) and (b) anodic oxidation process (peak d:  $\text{Li}_2\text{S} \rightarrow \text{S}_8$ ) versus the square root of the scan rates.

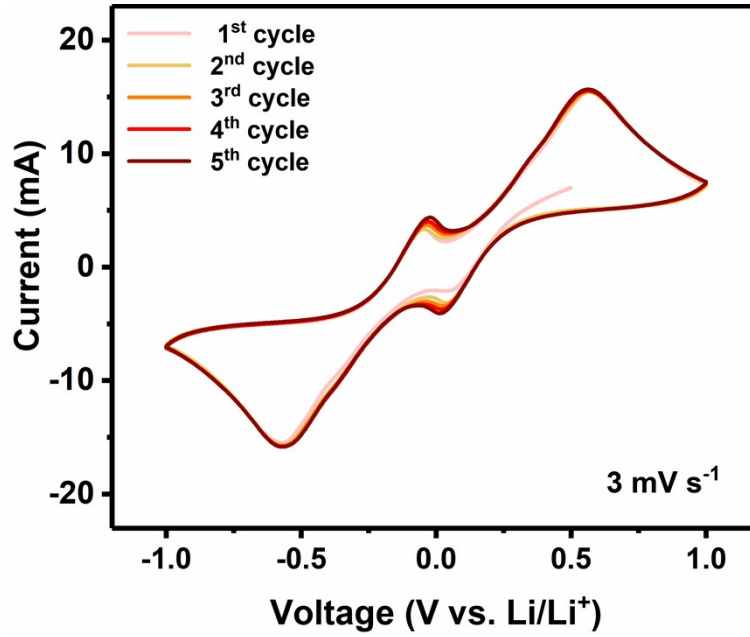


**Fig. S18** Multi-cycle voltammograms of the Fe/Fe<sub>3</sub>C@GNC symmetric cell at 3 mV s<sup>-1</sup>.

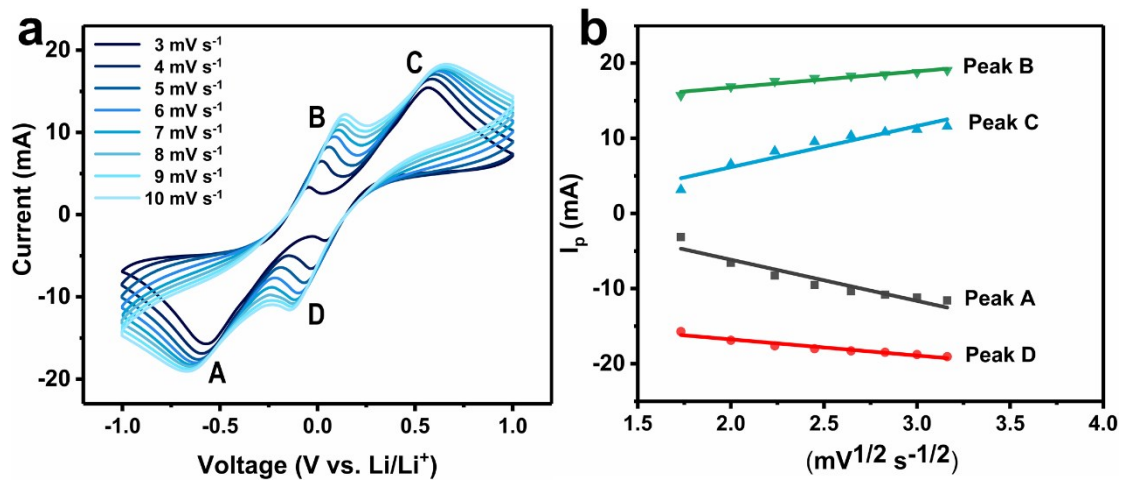


**Fig. S19** CV curves of the symmetric cells with Fe/Fe<sub>3</sub>C@GNC electrode at various scanning rates. (b) The corresponding CV peak current for the Fe/Fe<sub>3</sub>C@GNC symmetric cell vs the square root of the scan rates.

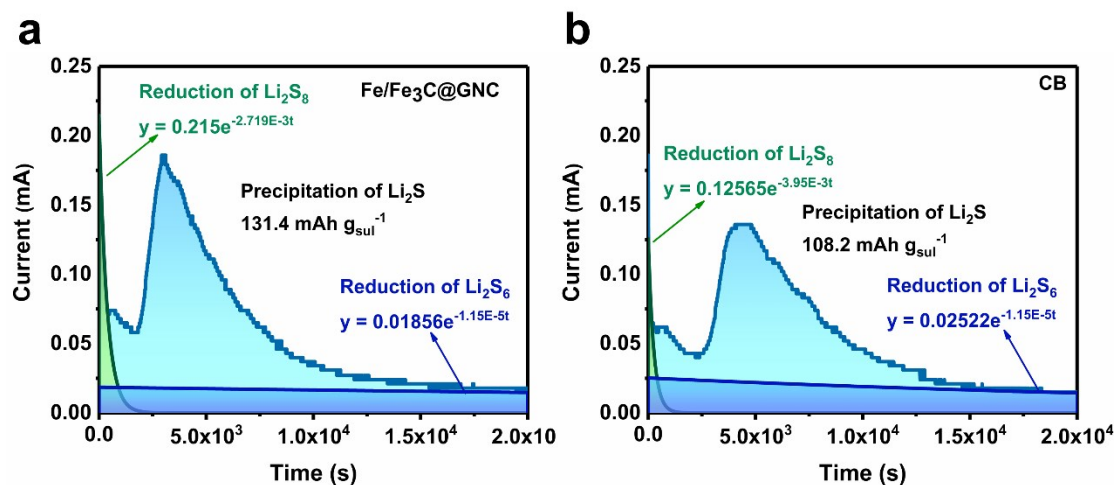


**Fig. S20** Potentiostatic discharge profiles of  $\text{Li}_2\text{S}_8$  solution at 2.05 V on the (a) Fe/Fe<sub>3</sub>C@GNC electrode and (b) CB electrode.

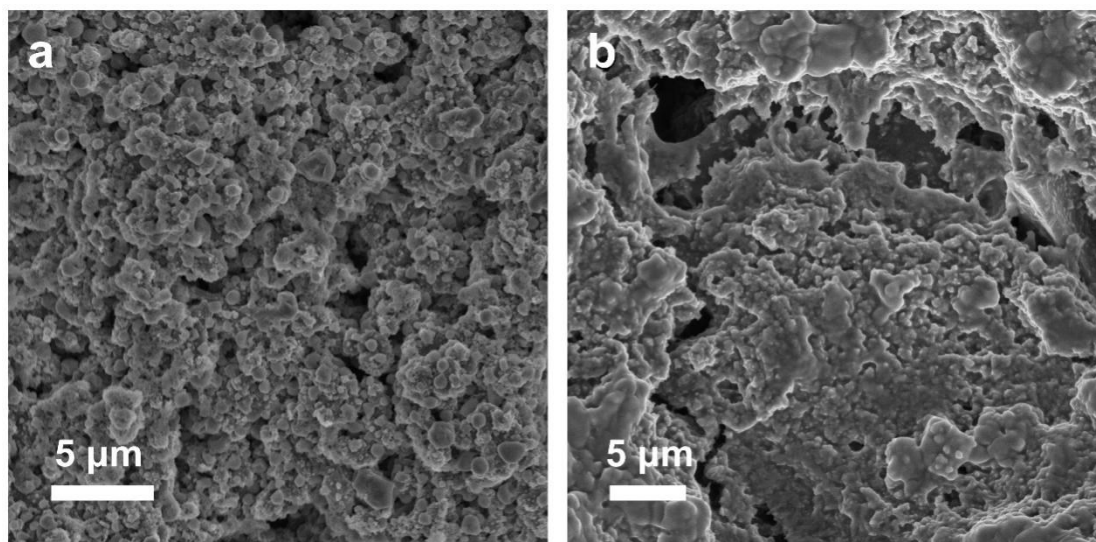


**Fig. S21** The SEM images of deposited  $\text{Li}_2\text{S}$  on (a) Fe/Fe<sub>3</sub>C@GNC and (b) CB working electrodes when current was down to  $10^{-5}$  A.

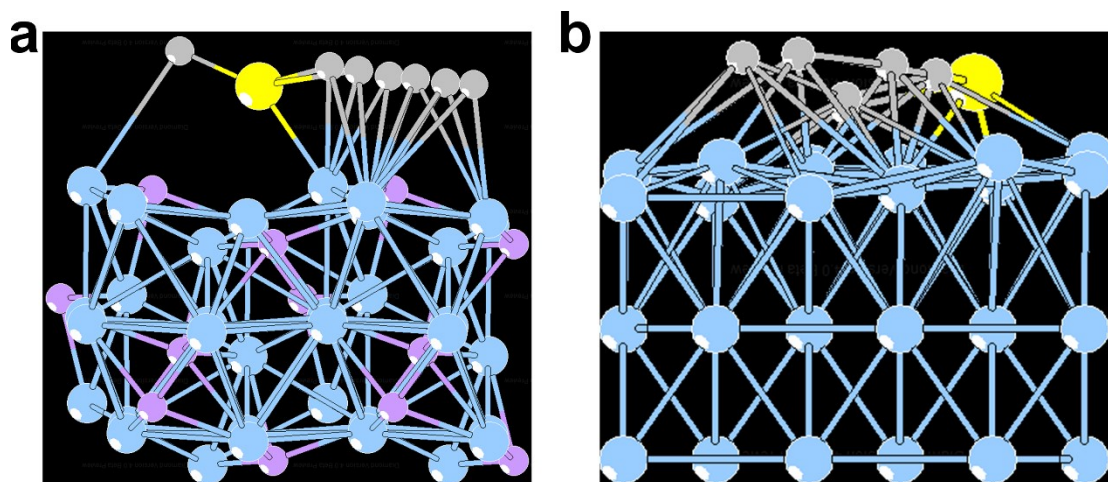


**Fig. S22** Optimized geometries of Li<sub>2</sub>S decomposition on the surface of (a) Fe<sub>3</sub>C (001) and (b) Fe (110). The Li, C, S, and Fe atoms are denoted by gray, purple, yellow and blue balls, respectively

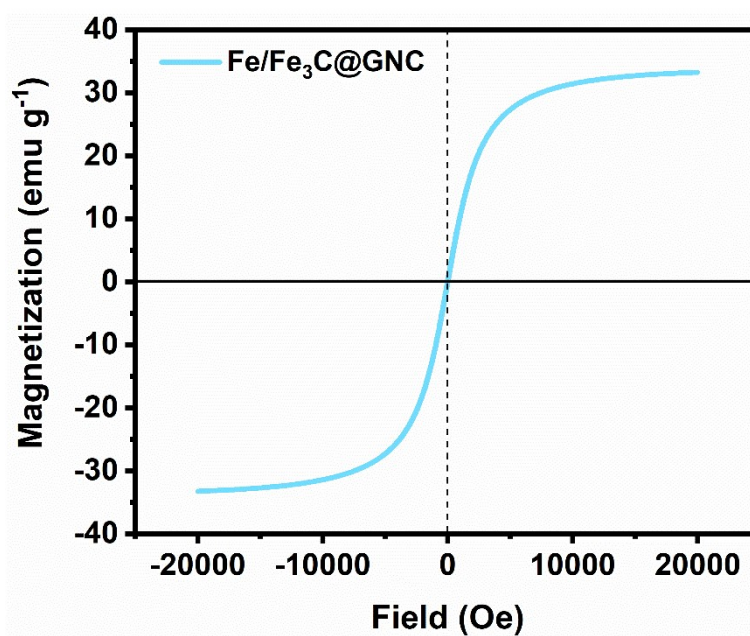


**Fig. S23** VSM curves of Fe/Fe<sub>3</sub>C@GNC composite.

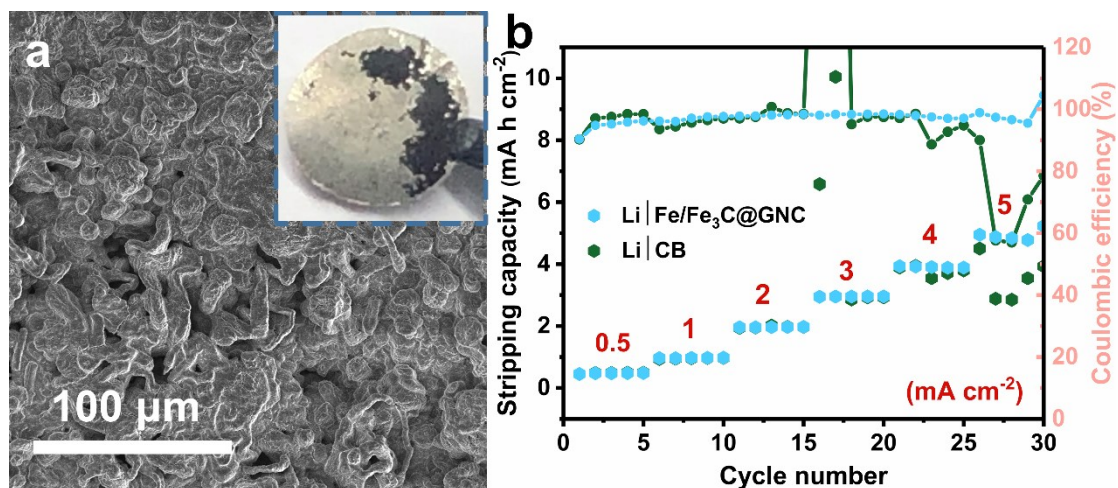


**Fig. S24** FESEM images of (a) CB electrode after depositing a capacity of  $3.0 \text{ mA h cm}^{-2}$  at a current density of  $0.5 \text{ mA cm}^{-2}$  with digital image in the inset. The rate performances of the Li|CB and Li|Fe/Fe<sub>3</sub>C@GNC cells. The plating time for each cycle is fixed to 1 h.

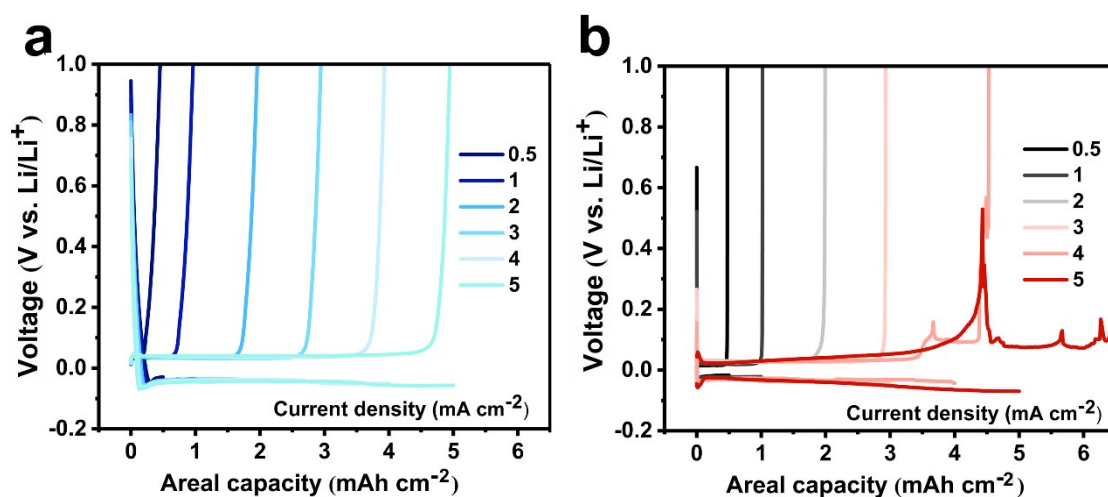


**Fig. S25** Selected discharge-charge curves of the (a) Li|Fe/Fe<sub>3</sub>C@GNC and (b) Li|Cu cells at different current densities ( $0.5\text{--}5.0 \text{ mA cm}^{-2}$ ).

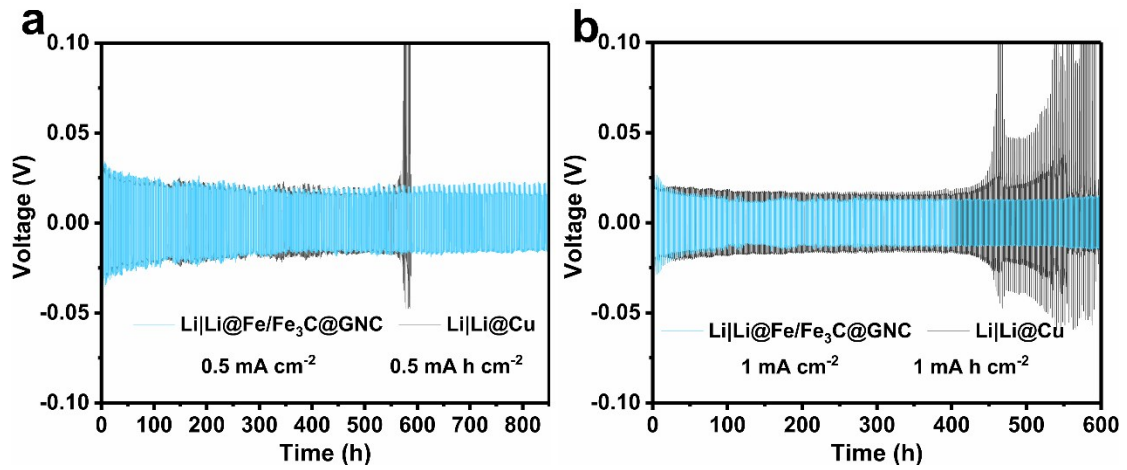


**Fig. S26** Voltage–time profiles of Li plating/stripping process at the current densities of (a)  $0.5 \text{ mA cm}^{-2}$  of  $0.5 \text{ mA h cm}^{-2}$  and (b)  $1 \text{ mA cm}^{-2}$  of  $1 \text{ mA h cm}^{-2}$  with pre-deposited Li of  $3 \text{ mA h cm}^{-2}$  in Li|Li@Cu and Li|Li@Fe/Fe<sub>3</sub>C@GNC symmetric cells.

**Table S1.** Atomic and mass ratio of carbon, nitrogen, oxygen and iron elements for Fe/Fe<sub>3</sub>C@GNC from EDS.

Element	Atomic %	wt%
C	81.38	72.51
N	10.06	10.43
O	6.25	7.41
Fe	2.32	9.63

**Table S2.** Comparison of electrical conductivity with previously reported carbonaceous materials.

Samples	Electronic conductivity (S cm <sup>-1</sup> )	References
Fe <sub>2</sub> O <sub>3</sub> -Fe <sub>3</sub> C/G/CNF	$1.17 \times 10^{-2}$	[6]
Fe <sub>3</sub> C/C	$8.24 \times 10^{-3}$	[7]
Fe <sub>2</sub> O <sub>3</sub> -graphene	$1.56 \times 10^{-1}$	[8]
Ni <sub>2</sub> -CPD <sub>py</sub> 973	$5.38 \times 10^{-2}$	[9]
GNC/Cas	$4.44 \times 10^{-1}$	[10]
GC-Fe-TiO	$3.9 \times 10^{-1}$	[11]
Starbon <sup>®</sup> A800	$8.4 \times 10$	[12]
NiO-GNS	$1.4 \times 10^{-3}$	[13]
CoS <sub>2</sub> /RGO-CNT	$7.2 \times 10^{-4}$	[14]
CB	$2.94 \times 10^{-2}$	This Work
Fe/Fe <sub>3</sub> C@GNC	$3.64 \times 10^4$ (5 MPa)	This Work

**Table S3.** EIS data of the batteries. R<sub>0</sub>: ohm resistance; R<sub>ct</sub>: charge-transfer resistance.

Samples	R <sub>0</sub> (Ω)	R <sub>ct</sub> (Ω)
Fe/Fe <sub>3</sub> C@GNC	2.369	10.43
CB	3.541	17.61
No interlayer	2.317	30.94

**Table S4.** Overpotential files of cells integrated with different interlayers.

Samples	$\Delta E_1$ (mV)	$\Delta E_2$ (mV)	$\Delta E_3$ (mV)
Fe/Fe <sub>3</sub> C@GNC	217.9	4.4	27.9
CB	346.9	7.5	5.6
No interlayer	291.4	47.5	19.5

**Table S5.** Onset potential of cells.

Samples	Onset potential (V)		
	Peak 1	Peak 2	Peak 3
Fe/Fe <sub>3</sub> C@GNC	2.488	2.090	2.078
CB	2.436	2.084	2.083
No interlayer	2.431	2.084	2.089

**Table S6.** The slope of the CV curve ( $I_p/v^{0.5}$ ).

Samples	Slope		
	Peak a	Peak b	Peak d
Fe/Fe <sub>3</sub> C@GNC	0.22919	0.44688	0.43454
CB	0.18371	0.18383	0.42393
No interlayer	0.17077	0.04152	0.30632

**Table S7.** Lithium ion diffusion coefficients derived from CV curves.

Samples	$D_{Li^+}$ ( $10^{-7}$ cm <sup>2</sup> S <sup>-1</sup> )		
	Peak a	Peak b	Peak d
Fe/Fe <sub>3</sub> C@GNC	0.70941	2.69703	2.55013
CB	0.45579	0.45639	2.42712
No interlayer	0.39385	0.02328	1.26723

## References

- [1] J. P. Perdew, K. Burke, M. Ernzerhof, *Phys. Rev. Lett.*, 1996, **77**, 3865.
- [2] G. Kresse, D. Joubert, *Phys. Rev. B*, 1999, **59**, 1758.
- [3] J.P. Perdew, K. Burke, M. Ernzerhof, Generalized Gradient Approximation Made Simple, *Phy. Rev. Lett.*, 77 (1996) 3865.
- [4] D.J. Chadi, Special points for Brillouin-zone integrations, *Phys. Rev. B*, 1977, **16**, 5188-5192.
- [5] L. Gong, D. Zhang, C.Y. Lin, Y. Zhu, Y. Shen, J. Zhang, X. Han, L. Zhang, Z. Xia, *Advanced Energy Materials*, 2019, **9**, 1902625.
- [6] C. Zhaoxia, J. Jingyi, C. Shengnan, L. Haohan, S. Min, Y. Mingguo, W. Xiaoxu and Y. Shuting, *ACS Appl. Mater. Interfaces*, 2019.
- [7] W. Kou, G. Chen, Y. Liu, W. Guan, X. Li, N. Zhang and G. He, *J. Mater. Chem. A*, 2019, **7**, 20614-20623.
- [8] J. Kan and Y. Wang, *Sci Rep*, 2013, **3**, 3502.
- [9] H. Nishihara, T. Hirota, K. Matsuura, M. Ohwada, N. Hoshino, T. Akutagawa, T. Higuchi, H. Jinnai, Y. Koseki, H. Kasai, Y. Matsuo, J. Maruyama, Y. Hayasaka, H. Konaka, Y. Yamada, S. Yamaguchi, K. Kamiya, T. Kamimura, H. Nobukuni and F. Tani, *Nat Commun*, 2017, **8**, 109.
- [10] W. Sun, A. Du, G. Gao, J. Shen and G. Wu, *Microporous and Mesoporous Materials*, 2017, **253**, 71-79.
- [11] Y. J. Hong, K. C. Roh and Y. C. Kang, *Carbon*, 2018, **126**, 394-403.
- [12] S. Kim, M. De bruyn, J. G. Alauzun, N. Louvain, N. Brun, D. J. Macquarrie, L. Stievano, B. Boury, P. H. Mutin and L. Monconduit, *Journal of Power Sources*, 2018, **406**, 18-25.
- [13] Y. Zou, Y. Wang, NiO nanosheets grown on graphene nanosheets as superior anode materials for Li-ion batteries. *Nanoscale* **3**(6), 2615-2620 (2011).
- [14] S. Peng, L. Li, X. Han, W. Sun, M. Srinivasan et al., Cobalt sulfide nanosheet/graphene/carbon nanotube nanocomposites as flexible electrodes for hydrogen evolution. *Angew. Chem. Int. Ed.* **53**(46), 12594-12599 (2014).